The structure of amylose gels

1994 J. Phys.: Condens. Matter 6 311

(http://iopscience.iop.org/0953-8984/6/2/003)

J. Phys.: Condens. Matter 6 (1994) 311–320. Printed in the UK

The structure of amylose gels

A M Vallêra†, M M Cruz†, S Ring‡ and F Boué§

† Departamento de Física, Universidade Lisboa, Campo Grande Edifício C1, 1700 Lisboa, Portugal

‡ AFRC Food Research Institute (Norwich), Colney Lane, Norwich NR4 7UA, UK

§ Laboratoire Léon Brillouin, Laboratoire Commun CEA-CNRS, CE de Saclay, 91191 Gif-sur-Yvette, France

Received 5 May 1993, in final form 20 September 1993

Abstract. Small-angle neutron scattering (SANS) has been used to study the gelation of amylose solutions in water in the range of concentrations of 2 to 8% by weight. The results clearly indicate a phase separation between polymer-rich and water-rich regions and an organization into a self-similar structure, with a characteristic fractal dimension of 2.6, independent of polymer concentration. The size and composition of polymer-rich aggregating units also show little dependence on the polymer concentration. A study of the gelation process leads to the conclusion that the fine structure of the gels, probed in this experiment, is independent of the cooling rate.

1. Introduction

Amylose gels have been the subject of various studies in recent years, but their structure is still not completely understood.

Amylose is one of the two main components of starch (along with amylopectin), and can be described as an essentially linear polysaccharide composed of α-(1 $\rightarrow$ 4) linked D-glucose.

Results from hydrodynamic studies indicate that this linear polymer behaves like a random coil in dilute neutral aqueous solution [1]. At room temperature, amylose solutions in water are unstable and, depending on concentration, can evolve in two different ways: if the concentration is smaller than $c^* \simeq 1$–1.5%, amylose precipitates; above this concentration, a milky and elastic gel forms [2, 3]. Gidley and Bulpin [3] and Clark *et al* [4] have shown that precipitation can be directly related to the degree of polymerization (DP) of the amylose. Using turbidity measurements and kinetic methods with monodisperse amylose, these authors have shown that precipitation is negligible for polymers with a DP > 1000, even for the lower concentrations used in their studies (1% in w/v).

The gelation of amylose has been studied by different techniques. Two main models have been proposed. Following Miles *et al* [5], the primary mechanism for amylose gelation is a phase separation between polymer-rich and polymer-deficient phases, with a subsequent development of crystalline zones in the polymer-rich region. Crystallization has been studied by I'Anson *et al* [6] using x-ray diffraction and was shown, for a polymer mass greater than 200 000, to be significant only a few hours after the gelation. In the second model, proposed by Gidley [7], amylose aggregation is due to cross-linking of long chains (chains in which the total chain length is substantially longer than the length involved in one interaction, of the order of 100 residues). Combining NMR and x-ray diffraction, he proposed that the gel has solid-like segments, present as aggregated double helices, that act as junction zones for

0953-8984/94/020311+10$07.50

the more mobile amorphous interjunction segments (single chains that behave like the ones found in solution).

Fourier IR studies [8] agree with both models, indicating the appearance of short-range order with the gelation process.

Neutron diffraction has the advantage of a large contrast between water and polymer and usually allows a clear interpretation of the results. In this paper we use small-angle neutron scattering (SANS) to help clarify the structure of amylose gels.

2. Experimental procedure

Amylose can be obtained in aqueous solution by the gelatinization of a suspension of starch granules, which results in the preferential solubilization of amylose. The amylose used in this study was obtained from pea starch (var. Filby). The process of isolation and characterization is described elsewhere [5]. Using light scattering, Miles *et al* [5] found that the amylose obtained in this way has an average gyration radius of 160 Å in dilute solution, and an average molecular weight of 500 000.

Aqueous solutions were made in D_2O in order to have good neutron scattering contrast between polymer and solvent and to decrease total incoherent scattering, thus improving the signal-to-noise ratio. Deuteration is not expected to alter the structure significantly, since gelation behaviour and temperatures are similar in deuterated and non-deuterated samples.

The amylose solutions used in these experiments had concentrations in the range of 2 to 8% by weight. They were prepared by heating a purified amylose (1-butanol) complex to 95 °C and removing the 1-butanol with a flow of heated nitrogen. The final concentrations were achieved by addition of heated D_2O and by bubbling the heated gas until the required volume was reached. Finally, the solutions were poured into 2 mm Hellman cells and divided into two different groups that followed different thermal histories.

Group 1—cooled to room temperature ($\simeq$ 25 °C) in steps of 5 °C at a controlled rate ($\simeq$ 0.5 °C min^{-1}); between each step the samples were maintained at constant temperature for about 30 min, during which measurements of the neutron scattered intensity took place.

Group 2—quenched from 90 °C to room temperature under cold running water.

The SANS experiments were performed on the PACE and PAXE diffractometers at the Laboratoire Léon Brillouin, CEA-CNRS, France. Details of the apparatus are described elsewhere [9].

The data were corrected and normalized against a water standard. In order to cover all the q-domain, sets of data were obtained with different neutron wavelengths and sample-to-detector distances. However, care was always taken to provide sufficient overlap for unambiguous merging of the different sets. For consistent overlap, it was necessary to use merging factors, typically 1.0 ± 0.2, for adjustment between different sets. This was true even for data obtained with different diffractometers, and suggests a confidence, in the absolute intensity, to $\simeq$ 20%.

Such critical points as the crossover behaviour evident in figure 1 were carefully studied; in particular, we verified that it was unequivocally observed within a single set of data, to make certain that no merging artifacts were involved.

3. Results and interpretation

3.1. Power laws

Typical results obtained in these experiments are shown in figure 1. Between 3×10^{-2} and the experimental limit of 2×10^{-3} Å^{-1}, the scattered intensity can be well fitted by a power law $I(q) = Aq^{-\delta}$ with $\delta = 2.6(1)$. This behaviour is characteristic of fractal structures [10] for which the structure factor is $S(q) \propto q^{-d_f}$; d_f is the fractal dimension and characterizes the relationship between mass content and size of a self-similar object. This q-dependence of the experimental intensity dominates in the low-q region, defined as $q \leqslant 2\pi/D$, D being the characteristic dimension of an aggregating unit. It therefore indicates scale invariance and a fractal structure with a fractal dimension of 2.6. In a real system this behaviour is also limited at low q by the dimension of the clusters, L, to $q \geqslant 2\pi/L$, a value still not obtained at the experimental limit of 2×10^{-3} Å^{-1}.

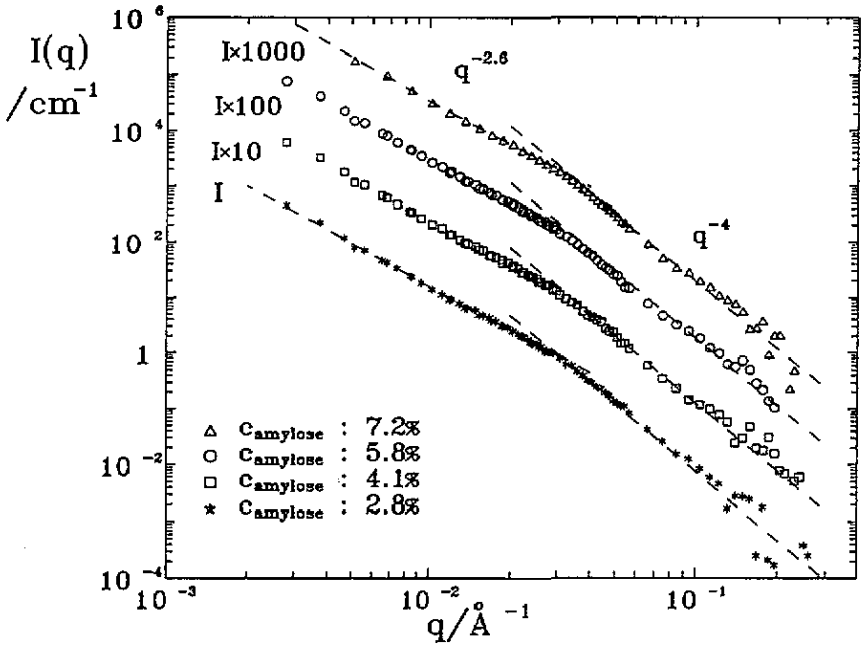

Figure 1. Small-angle neutron scattered intensity from amylose gels obtained for quenched samples. To avoid overlap, each set of data is displaced from the previous by a factor of ten. For all the gel concentrations presented, the two power laws discussed in the text are clearly visible.

We should remark that our data cannot be interpreted as due to 'particle scattering', as was done for previous results [6]. This becomes clear from consideration of an attempt to use a Guinier plot on our data (figure 2), which obviously does not exhibit independent particle behaviour.

Also, for all the range of concentrations studied, the results show a well defined Porod region $I(q) \propto q^{-4}$, extending from 3.5×10^{-2} to at least 2.5×10^{-1} Å^{-1}. This high-q behaviour is expected whenever there is a sharp interface between contrasting regions and consequently clearly indicates the existence, in the gel, of two phases with different polymer

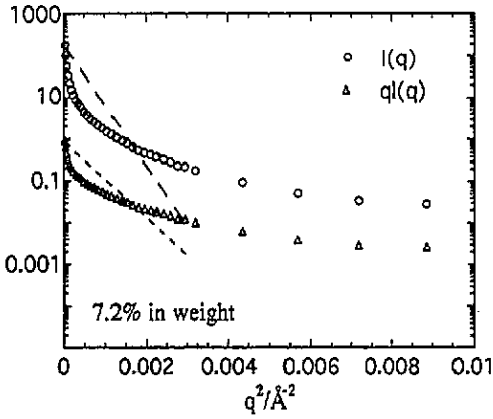

Figure 2. Guinier plots for a typical set of our results (quenched samples), assuming globular (○) or elongated (△) particles. $I(q)$ is given in absolute units. The data clearly fail to comply with Guinier behaviour for independent particles, which should be a straight line for $I(q)$ in the case of globular particles or a straight line for $qI(q)$ in the case of elongated particles. For comparison we draw the straight lines (broken) expected for independent particles, with the sizes deduced below (200 Å assuming globular particles and 130 Å assuming elongated particles), normalized to coincide with experiment at the lowest q.

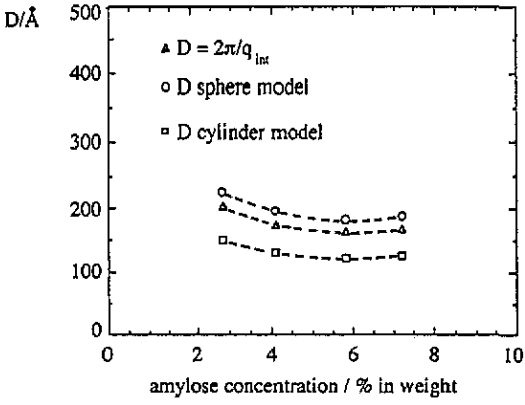

Figure 3. Typical dimension D of the aggregating unit obtained from the experimental results, as a function of amylose content (samples shown in figure 1): (*a*) from q_{int}, the q-intersection between the different regimes shown in figure 1, $D = 2\pi/q_{int}$ (△); (*b*) from the experimentally determined surface-to-volume ratio, and calculation of the diameter of aggregating spheres (○) or cylinders (□).

concentrations (these phases will be designated as polymer-rich and water-rich). The results therefore support the idea that amylose gelation is accompanied by a separation into two phases, confirming the previous results of Miles *et al* [5]. The emerging picture of the gels is that of a clearly separated polymer-rich phase, with a sharp interface with the water-rich region, which organizes itself as aggregated clusters of fractal structure.

3.2. Size of aggregating unit

In problems concerning fractal aggregation, most authors use models of simple aggregating particles, usually hard spheres. In our system, it is of course debatable whether an aggregating unit does exist. Still, the notion of a characteristic dimension of the objects that organize into a self-similar structure is certainly of interest.

One way of finding this characteristic dimension of an 'aggregating unit' is from the upper q-limit of the fractal regime as observed experimentally. We take this as the intersection of the straight lines fitted to the fractal and Porod regimes. These values of q, referred to as q_{int}, were determined for each of the four concentrations shown in figure 1 and are presented in table 1, together with other parameters directly obtained from the experimental results. The corresponding spatial dimensions, $2\pi/q_{int}$, are given in table 2.

Another independent way of calculating the average dimension of the aggregating units is to use the invariant

Table 1. Experimental parameters obtained for four of our samples as indicated in the text. Coefficient A is obtained from the fit of $I(q) = Aq^{-2.6}$ in the low-q region, and B from the fit of $I(q) = Bq^{-4}$ in the high-q region.

Amylose concentration (% by weight)	Pre-factor A, fractal region (cm^{-1} $Å^{-2.6}$)	Pre-factor B, Porod region (cm^{-1} $Å^{-4}$)	q_{int} ($Å^{-1}$)	Invariant Λ (cm^{-1} $Å^{-3}$)
2.8	1.00×10^{-4}	7.11×10^{-7}	0.0307	8.15×10^{-5}
4.1	1.54×10^{-4}	1.32×10^{-6}	0.0356	1.30×10^{-4}
5.8	1.92×10^{-4}	1.81×10^{-6}	0.0375	1.64×10^{-4}
7.2	2.16×10^{-4}	2.01×10^{-6}	0.0370	1.85×10^{-4}

Table 2. Characteristic dimension D of the aggregating unit deduced by two independent methods: (*a*) from the experimental volume-to-surface ratio $V_{p\text{-rich}}/\Sigma$, assuming spherical- or long-cylinder-like particles; and (*b*) from the end point of the fractal regime, q_{int}.

Amylose concentration (% by weight)	$V_{p\text{-rich}}/\Sigma$ (Å)	$D = 6V_{p\text{-rich}}/\Sigma$, sphere model (Å)	$D = 4V_{p\text{-rich}}/\Sigma$, long-cylinder model (Å)	$D = 2\pi/q_{int}$ (Å)
2.8	38.7	232	155	205
4.1	33.9	203	136	176
5.8	32.3	194	129	166
7.2	33.8	203	135	170

$$\Lambda = \int_0^\infty I(q)q^2\,dq = 2\pi^2(\rho_{w\text{-rich}} - \rho_{p\text{-rich}})^2\phi_1\phi_2 \tag{2}$$

and the coefficient of q^{-4} in the Porod region, known to be

$$q^4 I(q) = 2\pi(\Sigma/V)(\rho_{w\text{-rich}} - \rho_{p\text{-rich}})^2. \tag{3}$$

In these expressions, Σ is the total area of the interface, V is the sample volume, $(\rho_{w\text{-rich}} - \rho_{p\text{-rich}})$ is the contrast between the two regions with different polymer concentrations, and ϕ_1 and ϕ_2 are the volume fractions of polymer-rich and water-rich phases, respectively.

The ratio of these experimentally accessible quantities can be related to the volume-to-surface ratio of the polymer-rich phase. From this ratio we may obtain an estimate of the average diameter of the aggregating units, once we assume that they have a definite simple shape. For instance, in the case of monodisperse spheres of diameter D, $V_{p\text{-rich}}/\Sigma = D/6$; and, in the case of long cylinders, $V_{p\text{-rich}}/\Sigma = D/4$. From (2) and (3)

$$V_{p\text{-rich}}/\Sigma = V\phi_1/\Sigma = (\Lambda/q^4 I(q))1/\pi\phi_2 \tag{4}$$

Λ and $q^4 I(q)$ are determined experimentally, but ϕ_2 is not known precisely, since we ignore the exact water content in both phases. However, we may safely assume that the water-rich phase contains very little polymer, and since the polymer concentration is overall small, the error in estimating the volume fraction ϕ_1 will reflect little upon ϕ_2. The values for ϕ_2 actually used in this calculation took into account an estimate of the water content of the polymer-rich phase obtained from the absolute value of the invariant (see below); but an error of 100% here would reflect only $\sim 5\%$ in ϕ_2.

The results obtained using this method are presented in table 2.

The results of both methods, plotted in figure 3, are consistent. One should not give special significance to the 20% systematic difference, since a precise relationship between the two estimates would only make sense if we were to test a precise model for the shape and distribution of the aggregating units, which is outside of our aims here. The main conclusions we may deduce from consideration of figure 3 are that: (1) the typical 'diameter of a spherical aggregating unit' is of the order of 200 Å; and that (2) this is remarkably constant, showing little variation with polymer concentration in the solution. If, instead of spheres, one assumes the limit of long cylinders as the basic aggregating units, their typical diameter would be $\approx$ 135 Å. This is consistent with the network strands of diameter between 100 and 200 Å referred to by Leloup *et al* [11]. These strands were observed by electron microscopy in vitrified gel slices prepared by very rapid freezing.

3.3. Water content of the polymer-rich phase

The experimental data also allow an estimate of the composition of the polymer-rich phase, which may well be different from that of the crystalline phase of B-type amylose, described by Wu and Sarko [12] and Wild and Blanshard [13]. This is possible through the use of the invariant of equation (2) and a model for the composition dependence of volume fraction and neutron contrast. If we assume that the water-rich phase is just water, that the volume per water molecule in the polymer-rich phase is 30 Å^3, and take into account the lattice parameters for the B-type structure to estimate polymer volume, V_p, we obtain the following equations:

$$\phi_1 \simeq (1+x)V_p/V \tag{5}$$

$$\rho_{w\text{-rich}} - \rho_{p\text{-rich}} \simeq \rho_w - (\rho_p + x\rho_w)/(1+x) \tag{6}$$

where ρ_w and ρ_p are the estimated neutron scattering densities for water and polymer, and $x/(1+x)$ is the water volume fraction in the polymer-rich phase. Amylose residues were always assumed to have three OH groups with the same deuteration as the water.

Table 3. Polymer-rich phase composition obtained as number of water molecules per amylose residue. Crystalline amylose type-B has three water molecules per residue.

Water deuteration	*Amylose* concentration (% by weight)	*Water volume fraction* in polymer-rich phase $x/(1+x)$	*Water molecules* per residue
98%	2.8	0.44(4)	10
	4.1	0.39(4)	9
	5.8	0.44(4)	10
	7.2	0.46(4)	10
95%	2.8	0.29(5)	6
	4.1	0.20(6)	5
	5.8	0.35(5)	8
	7.2	0.40(5)	9

The results presented in table 3 clearly indicate a water content higher than that in B-type crystalline amylose, where only three water molecules are found per amylose residue. This is not surprising, since the polymer-rich phase is probably highly disordered. However, a precise estimate of the polymer-rich phase composition relies on the absolute value for

the scattered intensity and for the water deuteration. The imprecision in the scattered intensity was estimated as $\simeq 20\%$, from a comparison of results obtained in rather different experimental conditions. As for the water deuteration, the experimental procedure in sample preparation leads to a probable 98% deuteration. However, this was not controlled precisely, which increases substantially the imprecision of our calculation. In order to give an idea of the sensitivity to the degree of deuteration, in table 3 we also present the values corresponding to a 95% deuteration, considered as an already very improbable lower limit. We point out that for this low deuteration the internal consistency for the different concentrations, remarkable for 98%, is lost.

Our conclusion is therefore that our results are consistent with a composition of the polymer-rich phase independent of solution concentration, with an estimated 10(4) water molecules per amylose residue.

3.4. Polymer-rich/water-rich interface

The total interface area per unit volume can be obtained from the q^{-4}-coefficient (see equation (3)), once we have a value for the contrast. Table 4 indicates the values obtained assuming 98% water deuteration.

Table 4. Volume fraction of polymer-rich phase, ϕ_1, interface area per unit volume, Σ/V, and cluster size D_{cluster} (98% water deuteration was considered in both water and amylose OH groups for contrast calculation).

Initial solution concentration (% by weight)	ϕ_1	Σ/V (10^7 m^{-1})	D_{cluster} (μm)
2.8	0.051	1.33	35
4.1	0.076	2.47	11
5.8	0.108	3.39	4.3
7.2	0.134	3.76	2.6

The sharpness of the interface can be guessed from the high-q behaviour. The clear Porod region, extending from 3.5×10^{-2} Å^{-1} to at least 0.25 Å^{-1} (beyond this value statistical errors become too large), leads to the conclusion that the surface must be quite abrupt. In fact, a calculation for spheres with a 'thick' interface, where the scattered density varies linearly from $\rho_{\text{p-rich}}$ to ρ_{w} implied that the 'thickness' of the interface must be less than 15 Å, or else a shift from the Porod behaviour should have been experimentally observed.

3.5. Cluster size

We can also estimate the typical dimension of the clusters in the gel. This is fixed by the fractal dimension and the known overall polymer concentration in our samples. In fact, the polymer content M_{p} in a cluster of diameter D obeys $M_{\text{p}} \propto D^{d_{\text{f}}}$, and c_{p}, the polymer concentration, must obey $c_{\text{p}} \propto D^{d_{\text{f}}-3}$. Therefore, we must have, with $d_{\text{f}} = 2.6$

$$c^{\text{p}}/c^{\text{p}}_{\text{p-rich}} = c^{\text{p}}_{\text{cluster}}/c^{\text{p}}_{\text{unit}} = \phi_1 = (D_{\text{cluster}}/D_{\text{unit}})^{-0.4} \tag{7}$$

where $c^{\text{p}}_{\text{unit}}$ is the polymer concentration in the aggregating unit, assumed the same throughout the polymer-rich phase, and D_{unit} is the diameter of the aggregating units deduced from q_{int}. The values for D_{cluster} obtained from this relation are presented in table 4. These are of course theoretical estimates, obtained assuming that the fractal behaviour with $d_{\text{f}} = 2.6$ extrapolates all the way to these cluster sizes. They do predict, for all concentrations, the existence of inhomogeneities in the micrometer range, which explain the milky visual aspects of the gels.

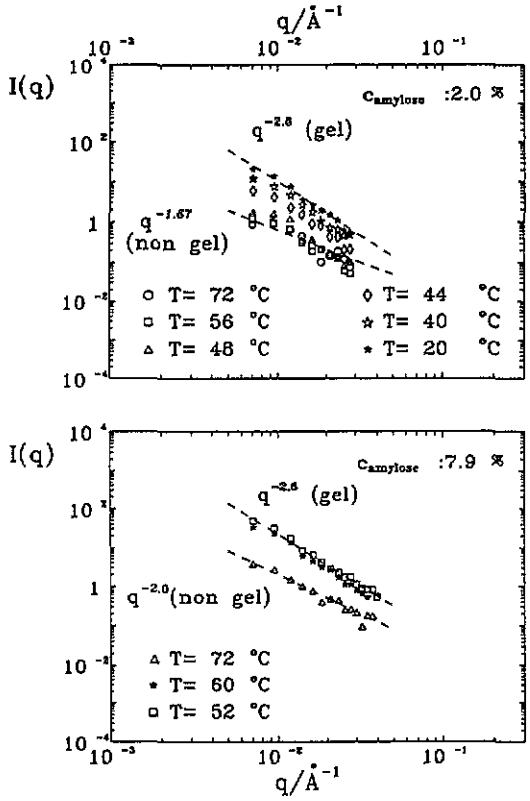

Figure 4. Evolution of the scattered intensity during the gelation process for two different concentrations (slowly cooled samples). The time intervals at each temperature were identical; the gelation velocity depends on the polymer concentration in the solution.

3.6. The gelation process

In figure 4 we present the evolution of the scattering intensity during the gelation of two samples. The evolution from the q-dependence of the polymer solution (shown to vary from $\simeq q^{-5/3}$ to $\simeq q^{-2}$, typical of dilute and concentrated solutions, respectively) to the characteristic $q^{-2.6}$ behaviour for the final gel is clearly demonstrated. The intermediate behaviour is concentration dependent and characterizes the gelation process. It shows that higher initial concentrations correspond to higher gelation temperatures for the same period of resident time, corroborating results obtained with other methods [4, 5]. For other concentrations, similar curves are obtained with systematic changes in the velocity and temperature at which gelation occurs.

No significant differences could be detected, in the q-range studied, between the gels obtained by rapid quenching (group 2) and the gels obtained by slow cooling (group 1), as shown in figure 5. Still, there was a visible difference in the turbidity: the quenched samples were more opaque than the slowly cooled ones. This implies a higher density of inhomogeneities at spatial frequencies that are efficient in scattering light, and therefore $I(q)$ for quenched and slowly cooled samples should differ in the μm^{-1} q-range. A possible speculation for this is that quenching does not allow full development of the clusters: there will be more of them, but smaller than in slowly cooled samples. These small clusters will not then fill all the sample volume, leaving macroscopic islands of pure water between them, which might well explain the increased turbidity.

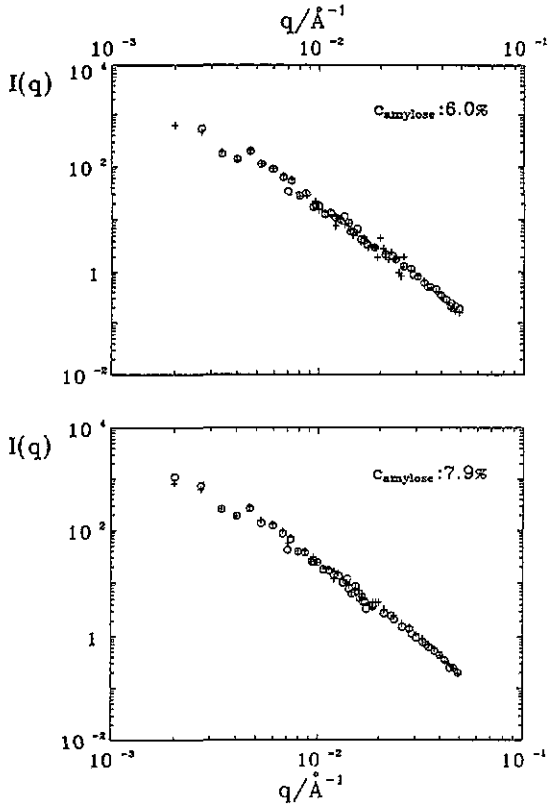

Figure 5. Comparison between scattered intensities for gels obtained with two different thermal histories: quenched samples (O) versus slowly cooled ones (+). The final structure seems independent of the cooling process for the range of spatial dimensions probed in our experiment.

4. Discussion and conclusions

Neutron scattering is known to provide clean results. However, for a complicated system like an amylose gel, we dare not expect such textbook simplicity as is patent in figure 1. Of course Nature can sometimes combine different effects in such a way as to induce erroneous conclusions from limited data; but it would then have to be mischievous indeed to provide such clear SANS data. This encouraged us to extract as much information as possible. Only the detailed shape of the crossover region was left out of the interpretation.

A very consistent picture of the structure of the amylose gels emerged. The polymer solution does separate into two phases during gelation, as shown by the Porod interface scattering, $I \propto q^{-4}$, at high q. The interface between contrasting regions is less than $\simeq$ 15 Å thick. This is quite abrupt, for it should be compared with the typical size of the polymer-rich phase units, which is of the order of 180 Å, as independently determined from the q at which crossover occurs and also from surface-to-volume ratios. Could the contrasting phases be ordered helix regions and water plus random amylose coils, as might be implied by some gelation models [7, 8]? In our opinion, no. The large volume occupied by the polymer-rich phase and the observed value for the contrast seem only consistent with one phase containing virtually all the polymer and quite a lot of water, estimated as $\simeq$ 43% in volume or $d \simeq 10$ water molecules per amylose residue, the other phase being virtually only water. This is not contradictory to their findings: the difference in interpretation results from the different scales probed. Whereas FTIR and NMR are sensitive to the close-range environment of bonds or ^{13}C nuclei, and are therefore good at probing

local order, at a few angstroms range, with SANS we probe correlations in the scale of $\simeq 20$ to $\simeq 2000$ Å. Local helix ordering is probably occurring, but within a polymer-rich phase, which also contains the very disordered coils. Our technique is not sensitive to the short-range fluctuations of density due to the contrast between small ordered regions ($\leqslant 20$ Å) and more disordered regions within that phase. (These could be detected, together with a more precise limit to interface abruptness, with longer counting times at the higher-q region, where presently statistical errors are too large.) Rather, it senses the remarkable contrast produced by objects $\simeq 180$ Å wide in a uniform medium. This characteristic size is little dependent on polymer concentration. These objects, as seen in the lower-q range (larger real space scale), are organized into a self-similar structure, with a fractal dimension $d_f = 2.6$, quite independent of polymer concentration. Similar fractal experiments are quite commonly found in dense polymer systems. The value obtained is close to the fractal dimension determined in solid particle aggregation [14], which agrees with the original Witten–Sanders model for diffusion-limited aggregation ($d = 2.5$ for three-dimensional systems [15]). We cannot, however, state that the mechanism behind the formation of this self-similar structure is of this kind.

Our study of the gelation process confirmed qualitatively the variations in velocity with polymer concentration and also the fast attainment of the final structure. No significant variations were detected in our diffraction data once the full gel structure was achieved—which, at room temperature, occurred too fast to be observed with our counting times. In this study, the most relevant, and perhaps surprising, result is that, within the range of our experiment, no difference could be detected between slowly cooled and very rapidly quenched gels. This means that the gel structure, up to the scale of $\simeq 2000$ Å, is the same, indifferent to cooling times from $\simeq 1$ s to $\simeq 1$ h.

Acknowledgments

We wish to acknowledge the support of the Cavendish Laboratory, Cambridge University, UK, to which one of the authors was affiliated during part of the work; and that of INIC, Portugal, and of the French Embassy in Lisbon, for their financial contribution.

References

[1] Banks W and Greenwood C T 1975 *Starch and its Components* (Edinburgh: Edinburgh University Press)
[2] Ellis H S and Ring S G 1985 *Carbohydr. Polym.* **5** 201
[3] Gidley M J and Bulpin P V 1989 *Macromolecules* **22** 341
[4] Clark A H, Gidley M J, Richardson R K and Ross-Murphy S B 1989 *Macromolecules* **22** 346
[5] Miles M J, Morris V J and Ring S G 1985 *Carbohydr. Res.* **135** 257
[6] I'Anson K J, Miles M J, Morris V J and Ring S G 1988 *Carbohydr. Polym.* **8** 45
[7] Gidley M J 1989 *Macromolecules* **22** 351
[8] Goodfellow B J and Wilson R H 1990 *Biopolymers* **30** 1183
[9] Laboratoire Léon Brillouin 1987 *Equipements Experimenteaux* (Gif-sur-Yvette: CEA-CNRS)
[10] Teixeira J 1988 *J. Appl. Crystallogr.* **21** 781
[11] Leloup V M, Colonna P and Ring S G 1990 *Macromolecules* **2** 862
[12] Wu H C and Sarko A 1978 *Carbohydr. Res.* **61** 7
[13] Wild D L and Blanshard J M V 1986 *Carbohydr. Polym.* **6** 121
[14] Sinha F K, Fraltoft T and Kjelm J 1984 *Kinetics of Aggregation and Gelation* ed F Family and D P Landau (London: Elsevier)
[15] Meakin P 1986 *On Growth and Form* ed H E Stanley and N Ostrowsky (Dordrecht: Martinus Nijhoff)